Plasma Chemistry and Plasma Processing, Vol. 24, No. 3, September 2004 (© 2004)

Molecular Beam Mass Spectrometry System for Characterization of Thermal Plasma Chemical Vapor Deposition

Soonam Park,[1] Feng Liao,[1] John M. Larson,[1,2] Steven L. Girshick,[1,3] and Michael R. Zachariah[1,3]

Received August 8, 2003; revised November 24, 2003

A molecular beam mass spectrometry system for in situ *measurement of the concentration of gas phase species including radicals impinging on a substrate during thermal plasma chemical vapor deposition (TPCVD) has been designed and constructed. Dynamically controlled substrate temperature was achieved using a variable thermal contact resistance method via a backside flow of an argon/helium mixture. A high quality molecular beam with beam-to-background signal greater than 20 was obtained under film growth conditions by sampling through a small nozzle (75 μm) in the center of the substrate. Mass discrimination effects were accounted for in order to quantify the species measurements. We demonstrate that this system has a minimum detection limit of under 100 ppb. Quantitative measurements of hydrocarbon species (H, H_2, C, CH_3, CH_4, C_2H_2, C_2H_4) using Ar/H_2/CH_4 mixtures and silicon species (Si, SiH, SiH_2, SiCl, $SiCl_2$, Cl, HCl) using Ar/H_2/$SiCl_4$ mixtures were obtained under thermal plasma chemical vapor deposition conditions.*

KEY WORDS: Thermal plasma; chemical vapor deposition; mass spectrometry.

1. INTRODUCTION

Thin films can be deposited by thermal plasma chemical vapor deposition (TPCVD) at rates one to three orders of magnitude higher than in conventional CVD methods. Unlike other more conventional CVD methods, TPCVD has some unique features: (1) freestream temperatures are in the thousands of K, (2) reactants are completely dissociated in the freestream, (3) the thermal boundary layer is very thin (~ 1 mm), and (4) the very thin boundary layer implies that the gas composition in the boundary layer deviates from equilibrium.[1] As a result, super-equilibrium concentrations

[1]Department of Mechanical Engineering, University of Minnesota, Minneapolis, MN 55455, U.S.A.
[2]Current address: Spinnaker Semiconductor, Eden Prairie, MN 55344, U.S.A.
[3]To whom correspondence should be addressed. E-mail: slg@umn.edu, mrz@me.umn.edu

0272-4324/04/0900-0353/0 © 2004 Plenum Publishing Corporation

of high enthalpy species lead to very high growth rates and interesting microstructures. Naturally growth rate and film quality are intimately connected to the nature and concentration of the depositing species, although the nature of the correlation is usually unknown.

Techniques have been developed to measure the spatially resolved species composition in reacting flows, and include laser-induced fluorescence (LIF), gas chromatography (GC), and molecular beam mass spectrometry (MBMS). LIF is well suited to detect radical species, but is generally not useful for stable species or molecules whose spectroscopy is not well known.[2] Furthermore the very thin boundary layer in TPCVD makes the use of a laser-based diagnostic in the boundary layer difficult. GC is a useful and reliable technique to detect stable species, however it is unable to measure unstable species. Larson *et al.*[1] used the GC technique to detect H_2, CH_4, C_2H_2, and C_2H_4 species during TPCVD of diamond films. Finally, molecular beam mass spectrometry (MBMS) is a powerful technique since it can detect both stable and unstable species, including radical species, and can measure a wide range of species simultaneously. Zachariah *et al.*[3] and Sanogo *et al.*[4] employed MBMS to sample from low-pressure flames and high temperature fast flow reactors to obtain elementary kinetic and mechanistic data. Toyoda *et al.*[5] applied the MBMS technique to measure stable species in low pressure chemical vapor deposition (LPCVD). Detailed MBMS sampling processes of chemical vapor deposition of diamond films have been investigated by Hsu *et al.*[6,7] Although the MBMS technique has been widely applied to combustion, and to low-pressure CVD and plasma systems, to our knowledge only one previous study[8] attempted to use MBMS in a thermal plasma system. The focus of that work was on measurement of methyl radicals during TPCVD of diamond. Unfortunately that work never succeeded in making measurements under diamond growth conditions, largely, we believe, because of the lack of substrate temperature control.

In this paper, we report on the development of an MBMS system designed to probe the chemistry of the TPCVD process under realistic deposition conditions, in a system that has been used to deposit silicon, carbon and silicon carbide films.[9] The operating characteristics of the MBMS system are discussed and examples from the deposition of carbon and silicon are presented.

2. DESIGN AND CONSTRUCTION

A well designed MBMS is a remarkably robust instrument in that it can provide a complete gas-phase analysis for a system. The essential feature of the method relies on the sudden transition from a continuum environment (a plasma in our case) to one that is collisionless. This sudden transition and

the associated creation of an ultra-cold supersonic molecular beam enables the preservation of the sample until it reaches an analytical device, which for MBMS is a mass spectrometer. The advantage of operating the source under continuum rather than effusive flow is that the intensities of molecular beams formed by the former are several orders of magnitude higher than by effusive flow. This effect results from the properties of gas dynamic expansions, where the hydrodynamic translational energy is increased, at the expense of random thermal, rotational, and to some extent, vibrational energy of the gas.[6,10]

2.1. TPCVD Reactor

Figure 1 shows a schematic of the TPCVD/MBMS system employed in this study. The TPCVD system is essentially operated in a stagnation flow

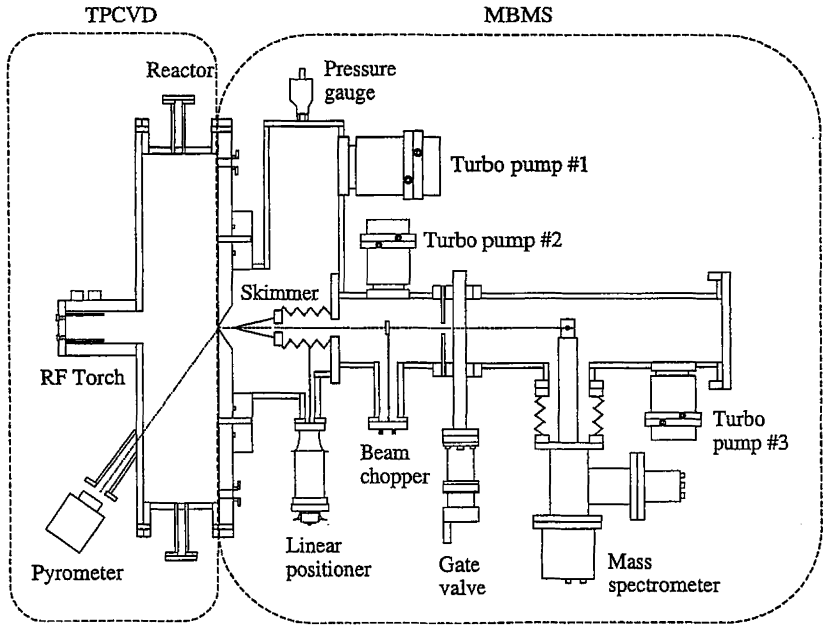

Chamber	Pressure, Pa	Orifice Size, mm
Source	2.7×10^{4}	
1st	1.3×10^{-1}	0.075
2nd	1.0×10^{-4}	1.0
Mass spec.	1.0×10^{-5}	1.5

Fig. 1. Schematic diagram of TPCVD/MBMS system.

deposition configuration. Major components include an inductively coupled 50-kW RF power generator operating at 3.2 MHz, a gas injection and metering system, and a substrate temperature control system (to be discussed later). An optical port enables optical pyrometry (~1.6 μm) for real-time determination of substrate temperature. The reactor pressure is maintained with a feedback pressure control system. Typical operating parameters include: gas flow rate of $Ar/H_2/CH_4$ (42.5 slm/2 slm/80 sccm) for carbon deposition, $Ar/H_2/SiCl_4$ (42.5 slm/1 slm/10 sccm) for silicon deposition, a reactor pressure of 20–33 kPa, a substrate temperature which was varied between 850 and 1150 K, and generator plate power of 10–15 kW. Figure 2 illustrates silicon film growth near the MBMS sampling orifice in the molybdenum substrate. Here we see that even at the lowest concentration of $SiCl_4$ used in our studies, the film growth rate is quite high (~60 μm/h) and in time results in plugging of the sampling orifice. This latter constraint has typically limited our MBMS run time to about one hour.

2.2. Creation and Detection of the Molecular Beam

The molecular beam is generated over three differentially pumped stages that include a movable skimmer and a tuning fork chopper to modulate the beam. Beam detection is accomplished with an electron impact ionizer and quadrupole mass filter mounted transverse to the beam. Because beam intensity is inversely proportional to the square of the length traveled we developed a nested design for the three chambers so as to minimize the distance between the substrate and the ionizer (37 cm).[11]

The first chamber downstream of the sampling orifice is pumped with a 1200 l/s turbomolecular pump to a nominal operating pressure under load of 0.13 Pa. An x–y movable conical skimmer with 1 mm diameter orifice and an apex angle of 30° is located approximately 1.0 cm downstream of the substrate. The orifice diameter and the angle of the skimmer were chosen to minimize skimmer interferences.[11] Since the ratio of the source pressure (P_o) to the background pressure in the first chamber (P_1) is quite high ($P_o/P_1 = 200{,}000$ in our case), we expect no intense shock waves, but rather a smooth transition from continuum to free molecular flow after the gas expansion.[12] This allows one to place the skimmer a little further back from the nozzle, and therefore in the free molecular flow regime, in order to promote efficient pumping behind the orifice. The skimmer chamber is pumped with a 250 l/s turbomolecular pump, and operated under sampling conditions at 1×10^{-4} Pa. After passing through the skimmer, the collimated molecular beam enters the mass spectrometer chamber through a 1.5-mm orifice drilled in a copper disk, that also serves as the sealing gasket separating the two chambers. The mass spectrometer chamber is nominally

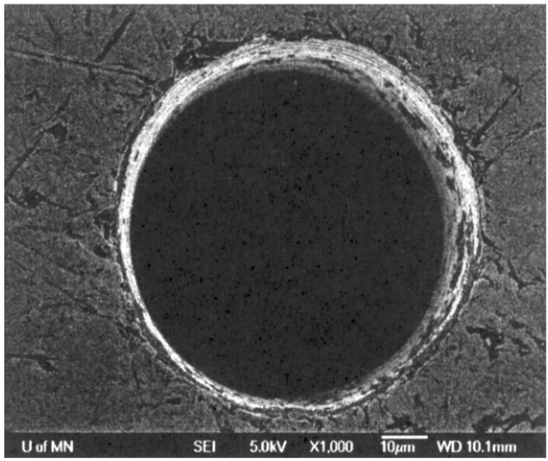

(a)

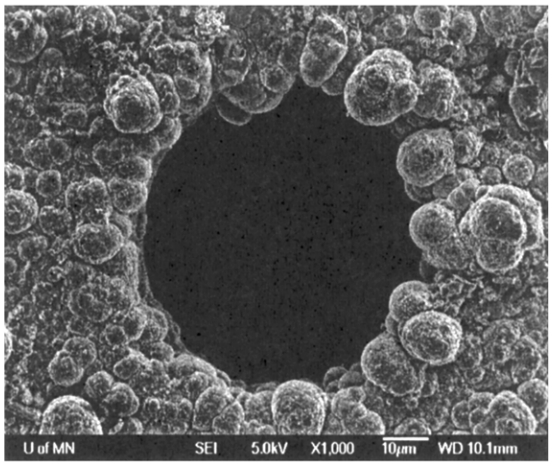

(b)

Fig. 2. SEM images of the orifice region of the molybdenum substrate (a) before film deposition. (b) post-deposition of silicon film. Deposition conditions: substrate temperature = 893 K, reactor pressure = 19.7 kPa, gas flow rate of $Ar/H_2/SiCl_4$ = 42.5 slm/1 slm/10 sccm, deposition time = 25 min.

operated at 1×10^{-5} Pa and is pumped by another 250 l/s turbomolecular pump. To eliminate hydrocarbon contamination from pump oil, a dry pump is used for backing the turbomolecular pump in the mass spectrometer chamber. The molecular beam enters a cross-beam-design variable energy electron impact ionizer, and the resulting ions are extracted into a quadrupole mass filter and detected with a secondary electron multiplier (SEM). To enhance signal-to-noise, a tuning fork chopper operating at 200 Hz is mounted between the skimmer and the ionizer, so that the modulated signal can be processed with phase-sensitive detection using a lock-in-amplifier.

Alignment of the substrate, skimmer, collimating, and ionizer orifices is accomplished with a He/Ne laser when the system is not under vacuum. Once the system is nominally aligned, final adjustments can be made while the system is under vacuum and the mass spectrometer is operating. The system was designed so that the skimmer position can be adjusted with an internal x–y movable stage. In addition, the ionizer/mass filter is housed in a chamber with a bellows, so that the whole chamber, and therefore the position of the ionizer, can be adjusted in three dimensions.

2.3. Sampling through the Substrate and Temperature Control

Our most difficult design challenge was to develop a substrate/sampling system that could simultaneously serve as a temperature-controlled substrate for CVD, while also providing a high-quality molecular beam source to probe the plasma boundary layer. A key requirement was the need not only to know the substrate temperature but also to be able to control it dynamically, and thus to maintain it constant, if desired, during an experiment. Unlike most CVD processes employing a separate substrate heater, for TPCVD the heat load from the plasma is so great that cooling of the substrate is required.

Given the high freestream temperatures and thin boundary layers in TPCVD it might seem surprising that one could expect relatively modest variations in substrate temperature to affect the gas phase chemical composition. However previous studies of TPCVD of diamond films, involving both gas chromatograph measurements and numerical modeling, demonstrated that varying substrate temperature by 100–200 K could significantly affect the chemical composition of gas arriving at the substrate. This is due to two effects. First, changing the substrate temperature changes the temperature profile in the boundary layer, which directly affects many gas phase reactions. Secondly, many surface reactions are sensitive to temperature, and this can strongly affect gas composition near the surface.

These design considerations led to a novel substrate assembly, consisting of three components: a sampling substrate, a spacer for dynamic control

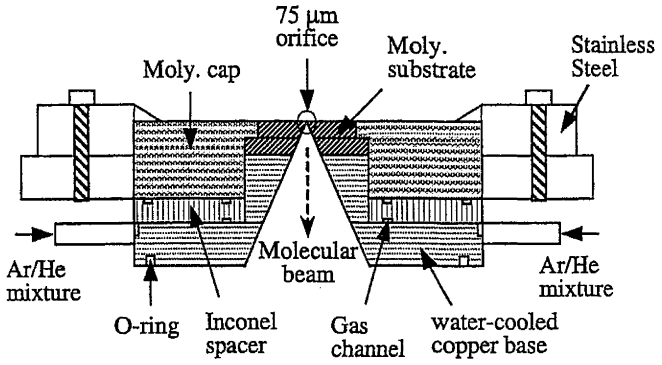

Fig. 3. Substrate assembly for MBMS sampling.

of the substrate temperature, and a water-cooled copper holder. Figure 3 shows a detailed drawing of the substrate assembly. The substrate is made of molybdenum, with a 75-μm-diameter orifice drilled in the center. The size of the orifice was constrained by the need to be large enough to sample under continuum conditions, in order to use the advantages of supersonic sampling, but not so large as to place an extreme requirement on pumping downstream of the orifice. The orifice should also have a small aspect ratio to reduce recombination of reactive species on the sidewalls. In our system, the length of the orifice channel is roughly equivalent to the orifice diameter (aspect ratio ≈ 1) with an internal angle of 68°. A viton o-ring at the bottom of the copper holder provides the vacuum seal. To maintain the desired substrate temperature, backside cooling is used. We employ gas channels of 1.5 mm diameter with an Inconel spacer in contact with a water-cooled copper holder. The purpose of the spacer and gas channels is to control the heat loss to the copper holder, by dynamically changing the thermal conductivity in the system by varying the mixture ratio of argon and helium that flows through the gas channels. Since the thermal conductivity of helium is approximately eight times that of argon, when used as an adjustable mixture, this method has previously been shown to provide controllable changes in overall thermal conductivity and therefore to accomplish temperature control of the substrate.[13]

2.4. Characterization of the MBMS System

2.4.1. Ionizer Calibration

One of the primary motivations for the implementation of MBMS is its ability to detect highly reactive species such as radicals. Unfortunately the nature of electron impact ionization is such that significant dissociation of

closed shell species (which usually exist in relatively high concentrations) can occur, resulting in the creation of dissociation products. For example, if our interest were in the detection of methyl radicals, and our ionizer was operated at 70 eV electron energy as is typically used, then, if any methane were present, we would detect methyl ions generated by the reaction $CH_4 + e \rightarrow CH_3^+ + H + 2e$.

Threshold ionization mass spectrometry (TIMS) takes advantage of the fact that the ionization potential for the radical, in this case the methyl radical, is usually lower than the appearance potential for the radical ion from the molecule, in this case methane. For example, the ionization potential for methyl is 9.8 eV, while the appearance potential for methyl ions from closed shell hydrocarbons is above 14.0 eV. By operating the ionizer at electron energy of 13.5 eV, one can thus screen out the contribution of methane to the methyl radical.

To use the threshold ionization technique it is necessary to accurately calibrate the electron energy output from the ionizer. Calibration was performed by extrapolating the QMS signal down to zero current using the known ionization cross-section for argon and linear extrapolation for helium and methane. The ionization cross-section of argon is given by:[14]

$$Q(E) = \begin{cases} 0, & E < 15.8\,\text{eV} \\ 3.18 \times 10^{-20} \ln\left(\dfrac{E}{15.8}\right) \dfrac{15.8}{E}, & E > 15.8\,\text{eV} \end{cases} \quad (1)$$

As shown in Fig. 4a, the intercepted threshold ionization energy equaled 18.8 eV, which is larger than the reference energy for argon (15.8 eV) by 3.0 eV. The intercepted threshold ionization energy of helium and methane was 2.6 and 4.0 eV greater, respectively, than that of their reference energies. Calibration over the whole cathode energy scale was obtained by a linear fit (Fig. 4b) of the measured threshold ionization energy with respect to the reference energy. All electron energies reported in this paper are those corrected by the calibration offset.

2.4.2. Quantitative Mole Fraction Analysis

In order to determine species mole fractions, one needs to relate the output from the QMS to gas concentrations at the sampling point. Since many of the physical parameters associated with molecular beam sampling and subsequent detection are difficult to model *a priori*, the usual practice is to make all measurements relative to an internal standard (usually a noble gas, e.g. Ar). It then becomes necessary to account only for those parameters in the system that are species dependent.

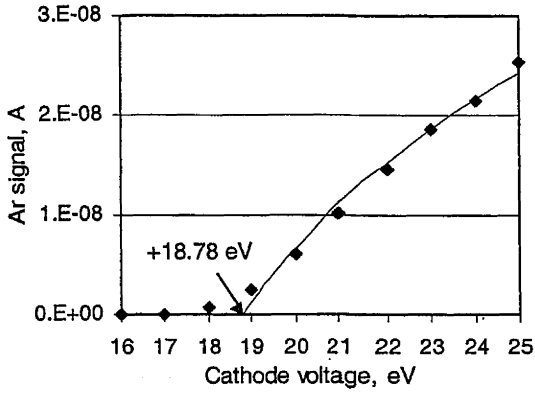

(a)

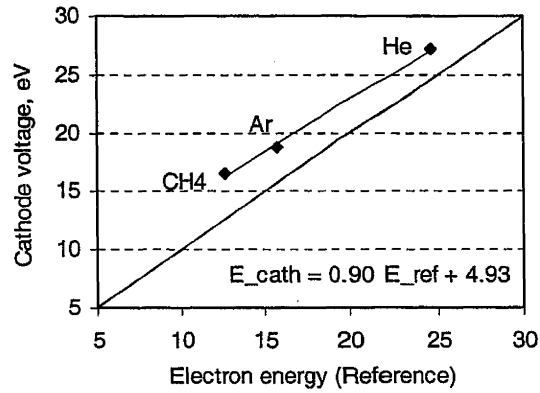

(b)

Fig. 4. Calibration of electron impact ionizer: (a) argon signal vs. cathode voltage. (b) cathode voltage vs. reference electron energy.

The mole fraction X of the ith species evaluated at the sampling point is given by

$$X_i = \left(\frac{I_i}{I_{\mathrm{Ar}}}\right)\left(\frac{\sigma_{\mathrm{Ar}}}{\sigma_{\mathrm{i}}}\right)\left(\frac{t_{\mathrm{Ar}}}{t_{\mathrm{i}}}\right)\left(\frac{a_{\mathrm{Ar}}}{a_i}\right)(X_{\mathrm{Ar}}) \tag{2}$$

where I_i and I_{Ar} are the detector currents for species i and argon, σ_i and σ_{Ar} are the ionization cross-sections evaluated at the appropriate electron

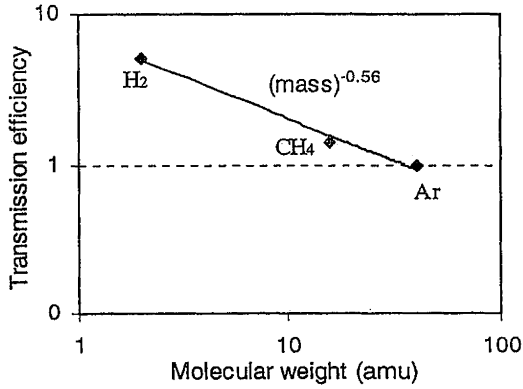

Fig. 5. Measured transmission efficiency through the quadrupole mass filter as a function of species mass.

energies, t_i and t_{Ar} are the transmission efficiencies of the quadrupole mass filter for a given mass-to-charge ratio, and a_i and a_{Ar} are the enrichment factors that account for the fact that heavy species, because of a smaller diffusivity tend to be enriched in the beam. Finally, we apply mass conservation.

$$\sum X_i = 1 \tag{3}$$

The transmission efficiencies (t_i in Eq. (2)) through the mass filter for particles of a given ion mass/charge depend on the electrostatic lenses and the resolution settings of the mass filter. It is therefore necessary to calibrate this parameter each time the spectrometer settings are changed. Once the electron energy scale is calibrated the mass filter transmission efficiencies are determined by introducing a known mixture of gases (H_2, CH_4, and Ar) directly to the mass spectrometer chamber through a leak valve. Figure 5 presents the transmission efficiency as a function of the species mass ($t \sim m^{-0.56}$) and shows the typical decrease in transmission efficiency with increasing mass/charge.

One of the properties of supersonic expansions from continuum flow is mass discrimination, i.e., the heavier gas species tend to enrich at the centerline of the molecular beam.[15–17] This effect can be caused by pressure diffusion, driven by the steep pressure gradient between the source pressure and the background pressure,[18] and by Mach-number focusing due to differences in thermal velocities between heavy and light species.[19] Skimmer interference and the scattering of the molecular beam with background molecules may also contribute to mass discrimination effects.[20,21] To determine the enrichment factor of the MBMS system we introduce a

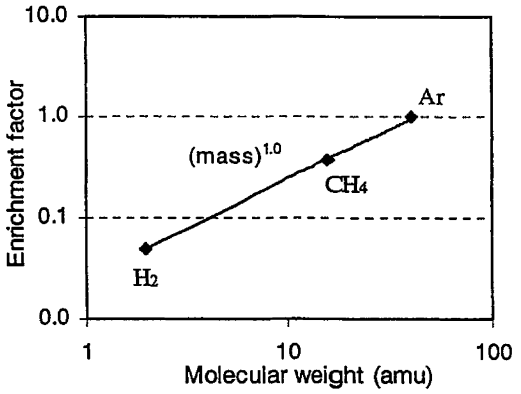

Fig. 6. Measured enrichment factor as a function of with the species mass. The reactor pressure = 19.7 kPa.

known gas mixture (H_2, CH_4, and Ar) into the reactor, so that we sample through the whole MBMS system. We also introduce the same mixture directly into the mass spectrometer. The enrichment factor is then obtained as follows:

$$a_i = \left(\frac{I_i}{I_{Ar}}\right)_{reactor} \Big/ \left(\frac{I_i}{I_{Ar}}\right)_{ms} \tag{4}$$

Figure 6 illustrates that the enrichment factor is linearly proportional to the mass ratio. For the case of continuum flow at the skimmer, Sharma *et al.*[19] argued that the enrichment factor should be linearly proportional to the mass ratio. As seen in Fig. 6, we found such a linear relationship to hold for our system, although we believe that in our system the flow at the skimmer is in the free molecular regime. This suggests that pressure diffusion at the source orifice, which can affect the enrichment factor for free molecule flow, is negligible in our system.

2.4.3. Beam Characteristics

During the continuum free jet expansion from the source at pressure P_o (in the reactor), to a lower pressure P_b (in the first chamber), the flow achieves sonic conditions at the orifice exit, and becomes supersonic as it expands into the chamber. Eventually the flow will equilibrate with the background pressure via a shock wave. The thickness of the shock wave, i.e. the Mach disk, is of order of the local mean free path, and its location,

X_m, can be approximated by[22]:

$$\frac{X_m}{d} = 0.67\left(\frac{P_o}{P_b}\right)^{0.5} \tag{5}$$

where d is orifice diameter. For our system ($P_o = 26.3$ kPa, $P_b = 0.13$ Pa, $d = 75$ μm) the calculated Mach disk location is about 2.2 cm downstream of the orifice exit, where the predicted pressure[12] is $\sim 10^{-6}$ Pa with a local mean free path over 50 cm. Since, however, the local mean free path is considerably longer than any characteristic skimmer dimensions in our system no shock structures should be formed.

To explain such a shock-free configuration, Miller[12] developed a "quitting surface model" so that rather than a shock separating the isentropic core from the background, he suggested that the isentropic continuum core be assumed to terminate (quitting surface) with a sudden transition to free molecular flow. He was able to develop an empirical relationship for the location of the quitting surface (X_{qs}):

$$\frac{X_{qs}}{d} \sim \left(\frac{M_\infty}{C_1}\right)^{1/(\gamma-1)} \tag{6}$$

For argon ($C_1 = 3.232$, $M_\infty = 1.17\ K\bar{n}_o^{0.4}$($Kn_o$ = Knudsen number at source conditions), $\gamma = 1.67$) the terminal Mach number (M_∞) in our system is estimated to be 7, and the location of the quitting surface is predicted to be 0.2 mm from the orifice, for a source temperature of 1000 K. Our skimmer is located 1 cm from the orifice, and is therefore well into the free molecular flow region.

The signal detected by the mass spectrometer is proportional to the gas density present at the ionizer, which is necessarily composed both of molecules arising from the molecular beam and of those molecules that comprise the background gas. In order to discriminate these two contributions, a tuning fork copper, that is amenable to phase-sensitive detection, was mounted between the skimmer and the ionizer. Also designed, for the purposes of modulating the molecular beam, was a mechanically operated flag that could be used to block the beam and provide a simple method to evaluate the beam quality. Figure 7 shows an example of such a measurement for argon during sampling from a plasma operating at 13.2 kPa. In this particular case, the ratio of the signal when the flag is open to that when it is closed, or what we refer to as the "beam-to-background ratio" is about 43, and indicates a strong molecular beam, with minimal skimmer interference. Figure 8a shows the characteristics of the molecular beam as a function of the reactor pressure under thermal plasma conditions. As the reactor pressure increases we see a monotonic increase in the background

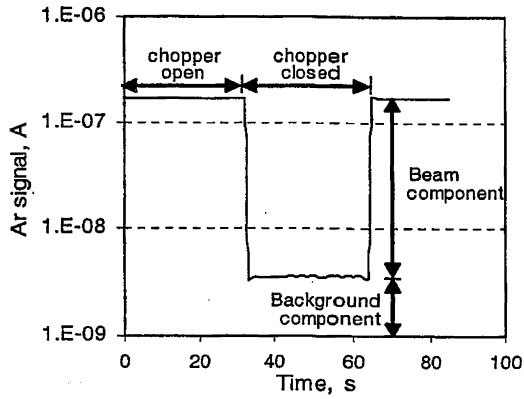

Fig. 7. Argon signal with chopper-open and chopper-closed under thermal plasmas conditions. The reactor pressure = 13.1 kPa.

signal as expected, since the load to the mass-spectrometer chamber, and hence the background pressure, increases. In contrast, the beam signal increases rapidly to a peak at ~20 kPa followed by a plateau or perhaps a slight decrease with increasing pressure. This behavior is characteristic of supersonic beams, and the decline is usually associated with skimmer interference effects and beam scattering by background molecules.[20] The beam-to-background ratio is shown in Fig. 8b, and indicates that we can obtain ratios well over 50 at pressures of about 6 kPa.

In summary, our MBMS system is capable of operating with reasonable beam quality for sub-atmospheric (20–40 kPa) thermal plasmas.

2.4.4. Sensitivity

To determine the ultimate sensitivity of our MBMS system we measured the signal from the isotopes of argon with a reactor pressure of 26.3 kPa at electron energy of 25 eV, as shown in Fig. 9. The minimum sensitivity was obtained by linearly extrapolating the beam signal down to a minimum current measurable by our detector (10^{-13} A). Figure 9 indicates a minimum sensitivity of 60 ppb for our system under optimal conditions.

3. RESULTS UNDER TPCVD CONDITIONS

We have measured hydrocarbon and silicon containing species, including radical species, under TPCVD conditions. For these studies the substrate temperature was varied from 905 to 1153 K at a fixed reactor pressure of 19.7 kPa.

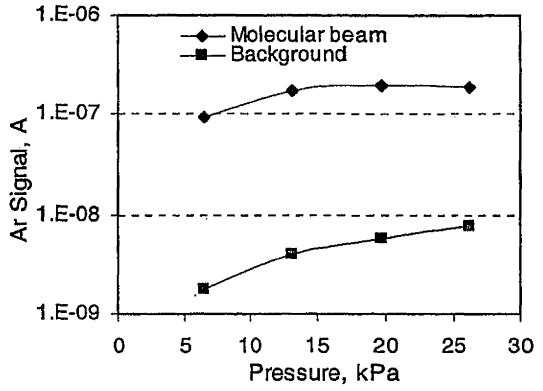

(a)

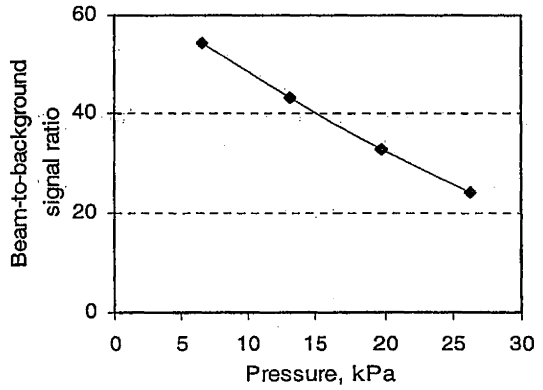

(b)

Fig. 8. Effect of reactor pressure on beam intensity and signal-to-background in an argon plasma: (a) argon molecular beam and background signal and (b) beam-to-background ratio with respect to reactor pressure. Substrate temperature = 940 K.

The selection of the time constant (τ) for the lock-in amplifier depends on the signal intensity of species under measurement. In most cases, except for argon, we operated with a time constant of 3 s. The sampling time (T) for a given species was then chosen as $T/\tau > 3$.[23] Electron impact ionization cross section data necessary to determine the mole fractions were mainly obtained from the NIST Web Database reference.[24] Ionization cross section data of Cl and HCl were obtained from Probst *et al.*[25] The NASA

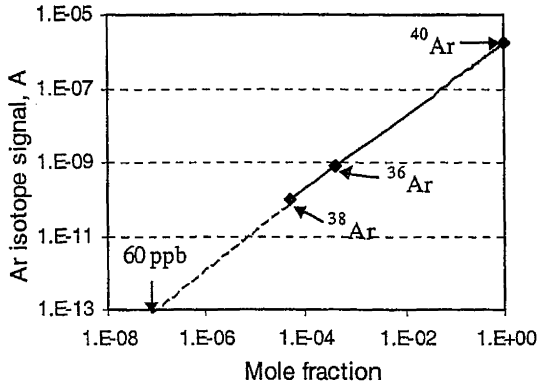

Fig. 9. Sensitivity determination of the MBMS system from argon isotope signals. Mole fractions of argon isotope are determined by Eq. (2). The minimum sensitivity of 60 ppb is obtained by extrapolating to 10^{-13} A.

AMES Research Center database[26] was used to obtain ionization cross sections for $SiCl_n$ ($n = 1$–4) species.

Feed gas flow rates of $Ar/H_2/CH_4$ for carbon deposition were 42.5 slm/2 slm/80 sccm and for silicon deposition the gas flow rates of $Ar/H_2/SiCl_4$ were 42.5 slm/1 slm/10 sccm. Table I and Table II present the working electron energies for the species measured. The measured mole fractions for hydrocarbon species and silicon species are shown in Figs. 10 and 11.

Table I. Ionization Potential (IP), Appearance Potential (AP) of Interfering Species, and Working Potential (WP) for Hydrocarbon Species Measurements

Species	IP (eV)	Interference	AP (eV)	WP (eV)
H	13.6	H_2	18.0	17.0
		CH_4	21.3	
		C_2H_2	18.8	
		C_2H_4	18.7	
H_2	15.4	C_2H_4	22.4	20.0
C	11.3	CH_4	19.6	18.0
		C_2H_2	20.4	
		C_2H_4	18.3	
CH_3	9.8	CH_4	14.3	13.5
		C_2H_4	17.0	
CH_4	12.6	C_2H_4	18.7	18.0
C_2H_2	11.4	C_2H_4	13.0	12.5
C_2H_4	10.5			11.5
Ar	15.8			25.0

Table II. Ionization Potential (IP), Appearance Potential (AP) of Interfering Species, and Working Potential (WP) for Silicon and Chloride Containing Species Measurements

Species	IP (eV)	Interference	AP (eV)	WP (eV)
H	13.6	H_2	18.0	17.0
H_2	15.4			20.0
Si	8.2			15.0
SiH	7.9	SiH_2	12.4	12.0
SiH_2	8.9			17.0
Cl	13.0	HCl	17.3	17.0
^{36}HCl	13.0	^{36}Ar		15.0
^{38}HCl	13.0	^{38}Ar		15.0
SiCl	8.6	$SiCl_2$	12.5	12.0
$SiCl_2$	10.9			17.0
Ar	15.8			25.0

In Fig. 10 we show the effect of substrate temperature on measured gas phase species concentrations above the substrate for an argon/hydrogen/methane plasma. The results indicate that acetylene (C_2H_2) is the most abundant hydrocarbon species. We also see that the mole fractions of C_2H_2, CH_4, and C_2H_4 tend to decrease as the substrate temperature increases from 905 to 1153 K. This result is consistent with Larson *et al.* (1999), who measured these species by gas chromatography.[1] The hydrogen atom concentration is seen to be in super-equilibrium concentrations relative to H_2 at the substrate temperature, implying that the gas-phase chemistry is not sufficiently fast relative to thermal transport processes to maintain equilibrium. The relative insensitivity of hydrogen concentration to substrate temperature is currently under investigation through the use of detailed chemical kinetic modeling.

We have also conducted measurements during silicon deposition from a argon/hydrogen/silicon tetrachloride plasma. The measurements of silicon and chlorine containing species are shown in Fig. 11. The mole fractions of atomic Cl and HCl are determined from a sum of ^{35}Cl ($m/e = 35$) and ^{37}Cl ($m/e = 37$) isotopes. To measure the mole fraction of $H^{35}Cl$ ($m/e = 36$) and $H^{37}Cl$ ($m/e = 38$) we use an electron energy of 15 eV, which is below the ionization potential of argon, so as to screen out contributions from ^{36}Ar and ^{38}Ar. Atomic silicon was observed to be the dominant silicon-containing species, while hydrogen chloride (HCl) is the dominant chlorine-containing species. In general silicon hydride species were found to be in higher concentration than silicon chloride species, as expected given the greater stability of the Si–H bond.

The uncertainty of our measurements can be determined from the combined contributions of calibration and measurement errors. The main contribution to the calibration error is uncertainty in the reported ionization

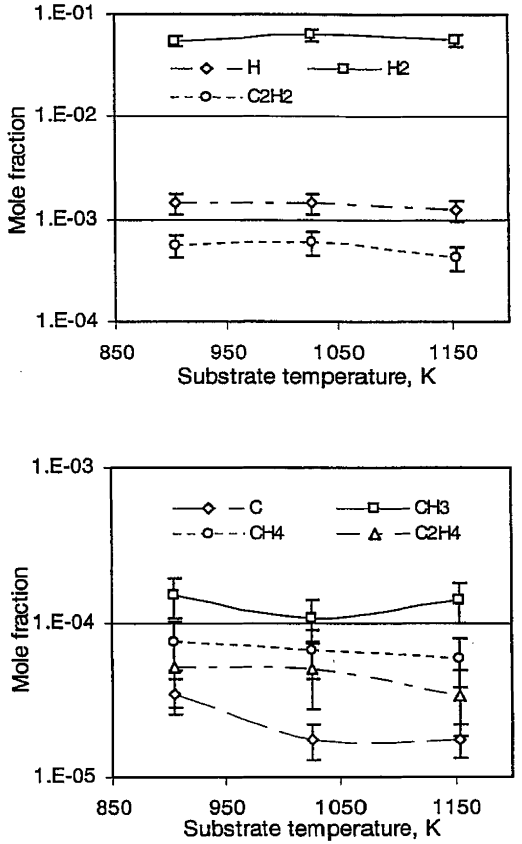

Fig. 10. Measured mole fractions of hydrocarbon species as a function of the substrate temperature in a thermal plasma. Feed gas flow rates of $Ar/H_2/CH_4$ are 42.5 slm/2 slm/80 sccm. Reactor pressure = 19.7 kPa.

cross section data, estimated to be ±10%. The measurement uncertainty can be calculated as the standard deviation in the individual species measurements. The overall uncertainty for all the species measured and computed in this way was found to be less than 50%.

4. CONCLUSION

We describe the design and operation of a molecular beam mass spectrometry system capable of quantitative measurement of gas phase species (stable and radical) sampled through an orifice in a temperature-controlled substrate during thermal plasma chemical vapor deposition. The system is capable of operating with large beam strengths (beam-to-background > 20),

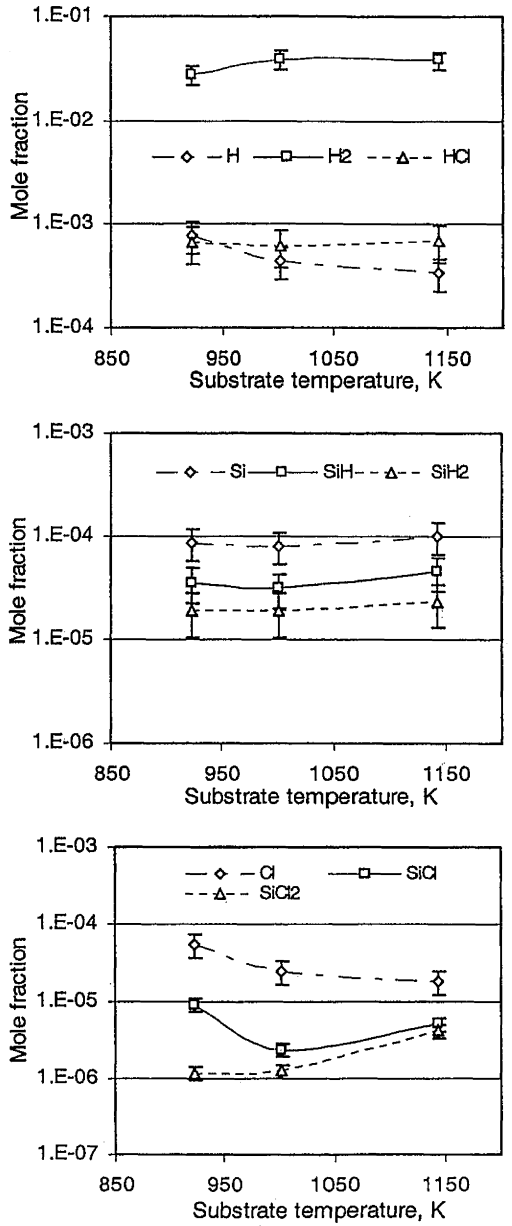

Fig. 11. Measured mole fractions of silicon and chlorine containing species as a function of substrate temperature during silicon plasma deposition. Feed gas flow rates of $Ar/H_2/SiCl_4$ are 42.5 slm/1 slm/10 sccm. Reactor pressure = 19.7 kPa.

up to pressures of 30 kPa. With the use of threshold ionization and appropriate corrections for mass discrimination, we have demonstrated the ability of the instrument to quantitatively measure radical species, and under optimal conditions at sensitivity below 100 ppb. We demonstrate the application of the instrument during the deposition of silicon and carbon films as a prelude to our subsequent studies to characterize the formation of silicon carbide and boron carbide films.

ACKNOWLEDGMENTS

This research was partially supported by the National Science Foundation under grant CTS-9910718 and by the Minnesota Supercomputing Institute.

REFERENCES

1. J. M. Larson, M. T. Swihart, and S. L. Girshick, *Diamond Relat. Mater.* **8**, 1863 (1999).
2. M. R. Zachariah and D. Burgess Jr., *J. Aeros. Sci.* **25**, 487 (1994).
3. M. R. Zachariah and O. I. Smith, *Combust. Flame* **69**, 125 (1987).
4. O. Sanogo and M. R. Zachariah, *J. Electrochem. Soc.* **144**, 2919 (1997).
5. H. Toyoda, H. Kojima, and H. Sugai, *Appl. Phys. Lett.* **54**, 1507 (1989).
6. W. L. Hsu and D. M. Tung, *Rev. Sci. Instrum* **63**, 4138 (1992).
7. W. L. Hsu, M. C. McMaster, M. E. Coltrin, and D. S. Dandy, *Jpn. J. Appl. Phys.* **33**, 2231 (1994).
8. P. G. Greuel, J. T. Roberts, and D. W. Ernie, in *Proc. 12th Int. Symp. Plasma Chemistry*, Minneapolis, 21–25 August, 1995, Vol. 3, p. 2209.
9. F. Liao, S. Park, J. M. Larson, M. R. Zachariah, and S. L. Girshick, *Mater. Lett.* **57**, 1982 (2003).
10. A. Kantrowitz and J. Grey, *Rev. Sci. Instrum.* **22**, 328 (1951).
11. E. L. Knuth, *Engine Emissions: Pollutant Formation and Measurement* (G. S. Springer and D. J. Patterson, eds.), Plenum, New York, 1973, pp. 319–363.
12. D. R. Miller, *Atomic and Molecular Beam Methods*, Vol. 1 (G. Scoles, ed.), Oxford University, New York, 1988, Chap. 2.
13. M. T. Bieberich and S. L. Girshick, *Plasma Chem. Plasma Process.* **16**, 157S (1996).
14. M. Mitchner and C. H. Kruger, *Partially Ionized Gases*, John Wiley & Sons, 1973, p. 112.
15. J. B. Anderson, *AlChE J.* **13**, 1188 (1967).
16. P. C. Wateraman and S. A. Stern, *J. Chem. Phys.* **31**, 405 (1959).
17. V. H. Reist and J. B. Fenn, *J. Chem. Phys.* **39**, 3240 (1963).
18. F. S. Sherman, *Phys. Fluids* **8**, 773 (1965).
19. P. K. Sharma, E. L. Knuth, and W. S. Young, *J. Chem. Phys.* **64**, 4345 (1976).
20. E. L. Knuth, *Combust. Flame* **103**, 171 (1995).
21. J. B. Anderson, *Molecular Beam and Low Density Gas Dynamics* (P. P. Wegener, ed.), Dekker, New York, 1974, Chap. 1.
22. H. Ashkenas and F. S. Sherman, *Rarefied Gas Dynamics*, Vol. 2 (J. J. de Leeuw, ed.), Academic Press, New York, 1966, pp. 84–105.
23. S. S. Dijulio and E. L. Knuth, *Rev. Sci. Instr.* **55**, 1154 (1984).

24. Electron-Impact Ionization Cross Sections Database, NIST, http://physics.nist.gov/PhysRefData/Ionization/Xsection.html.
25. M. Probst, H. Deutsch, K. Becker, and T. D. Mark, *Int. J. Mass Spectrom. Ion Proc.* **206**, 13 (2001).
26. Electron Collision Cross sections and Databases, http://www.cfdrc.com/~cfdplasma/NASA_coll.html.